

Multifractal metal in a disordered Josephson Junctions Array

M. Pino,¹ V. E. Kravtsov,^{2,3} B. L. Altshuler,⁴ and L. B. Ioffe^{5,6}

¹*Instituto de Física Fundamental, IFF-CSIC, Calle Serrano 113 b, Madrid E-28006, Spain.*

²*Abdus Salam International Center for Theoretical Physics, Strada Costiera 11, 34151 Trieste, Italy*

³*L. D. Landau Institute for Theoretical Physics, Chernogolovka, Russia*

⁴*Physics Department, Columbia University, 538 West 120th Street, New York, New York 10027, USA*

⁵*CNRS and Université Paris Sud, UMR 8626, LPTMS, Orsay Cedex, F-91405, France*

⁶*National Research University Higher School of Economics, Moscow, Russia*

We report the results of the numerical study of the non-dissipative quantum Josephson junction chain at high temperatures. The disorder in this chain is due to the random offset charges. This chain is one of the simplest physical systems to study many body localization. We show that at high temperatures the system exhibits three distinct regimes: insulating, characterized by the full localization of many body wave function, fully delocalized (metallic) one characterized by the wave function that takes all available phase volume and the intermediate regime in which the volume taken by the wave function scales as a non-trivial power of the full Hilbert space volume. In the intermediate, non-ergodic regime the generalized conductance does not change as a function of the chain length indicating a failure of the conventional one parameter scaling theory of localization transition. The local spectra in this regime display the fractal structure in the energy space.

Introduction. The concept of single particle localization introduced by Anderson in 1958 [1] was in fact prompted by the experiments of Fehrer [2] that studied electron spin relaxation of P dopants in Si, a typical many body problem. Despite its conceptual importance, the many body localization remained out of limelight until the paper that [3] proved the existence of disorder driven transition in many body systems. In contrast to the single body localization, the properties of localization in the Fock space of many body system remain controversial. In particular, it is very well established that single particle localization in three dimensional space happens as a result of a single transition. Only at the transition point the properties of a single particle wave function are described by the scaling laws with anomalous dimensions [4]. Recently it was proposed [5] that this simple picture does not hold for many body localization: the many body wavefunction retains anomalous dimensions in a finite parameter region. In this region, the volume occupied by a typical wave function scales as anomalous power of the full Hilbert space volume that continuously changes from $D = 0$ in the insulator to $D = 1$ in a fully delocalized state. In a qualitative agreement several groups have found that the dynamics in this region is often described by non-trivial power laws that are neither diffusive nor localized [6–8].

The anomalous dimension of the wave function implies that a many body system does not visit all allowed configurational space in the course of time evolution, i.e. non-ergodicity. Below we shall refer to the state in which $0 < D < 1$ as non-ergodic state. Qualitatively, the appearance of such state is very natural in strongly disordered quasiclassical systems where strong disorder prevents the system from visiting all Hilbert space while the quasiclassical parameter makes localization very difficult. Empirically such behavior is well known for spin glasses

with large spin that break ergodicity without full localization. The possibility of a non-ergodic state would be very important for the interpretation of the experiments on atomic systems such as [9] because it implies that slow dynamics does not mean full localization.

This existence of a non-ergodic regime gets additional support from the results [10–12] for the single body localization on Cayley tree and random regular graphs, the problems that are believed [3, 13] to be similar to the many body localization. Even though there is no doubt that single particle localization on Cayley tree displays the non-ergodic behavior, the applicability of this result to many body problems and even to random regular graphs was questioned recently [14–16]. Unlike the single particle problem on the Cayley tree the full many body localization does not allow analytical treatment, so one has to resort to numerical analysis that remain inconclusive for available system sizes, with some workers preferring ergodic Griffiths phases [17, 18] while others fractal non-ergodic regime [15, 19–21]. The difficulty with the interpretation of the data is partly due to the fact that the non-ergodic regime appears in a narrow range of parameters in the models studied by these works.

In this paper we report the evidence for the appearance of a wide non-ergodic regime in the model where this regime is expected to appear in a wide range of parameters. Qualitatively, one expects that this situation is realized in the systems with large quasiclassical parameter in which the localization is driven by another parameter that can be changed independently.

One expects that the wave function in the non-ergodic state can be visualized as hybridization of distant resonances that happen to be very close in energy, see Fig. 1. It is in this respect that the many body problem differs from the single body: in the former the number of states grows exponentially with the order of the per-

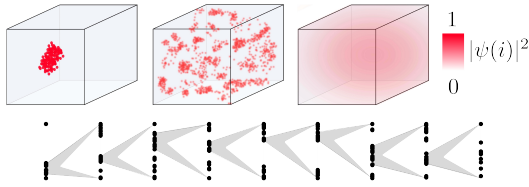


FIG. 1. Upper panel - cartoon of a many body wave function in three distinct regimes localized (left), non-ergodic metallic and ergodic states (right). These regimes differ by the ratio of the total number of Fock states, N , and the support set Ω , where wave function is significant. In a localized state, the volume of the support set, Ω is finite, or at most logarithmic, so $\Omega/N < \ln(N)/N$. For the non-ergodic metal the support set forms a fractal structure, so $\Omega/N < N^{-\nu}$ with $\nu < 1$. In the ergodic phase, the support set scales with the dimension of the Many-Body space, so $\Omega/N \sim 1$ and the probability is uniform. Low panel - the local spectrum (energy levels for which wave function is significant on a given site) is similar to the random Cantor set. The full spectrum (left) contains 5000 energy levels forming groups separated by large gaps. Zoom into each group produces similar structure at all energy scales.

turbation theory that makes it likely to find very distant weakly coupled but strongly mixed resonances. The states formed by the linear combinations of these resonances form a *mini-band* that is responsible for delocalization. All energy scales in this mini-band are small and determine the Thouless energy, E_{Th} , for the whole system that might become much less than average level spacing so that the effective many body conductance $g = E_{Th}/\delta \ll 1$ and size independent in a wide parameter range. Our numerical results shown below confirm this qualitative picture.

The formation of mini-bands characterized by small Thouless energy can be viewed as a consequence of weak interaction strength which is nevertheless sufficient for delocalization. This unusual regime is known to occur in critical power-law banded matrices with parametrically small off-diagonal elements $\langle H_{nm}^2 \rangle = b^2/(n-m)^2$ with $b \ll 1$ [22]. In this model the dimensionless conductance turns out to be small $g \sim b$ and size independent at the transition.

The conductance that varies by orders of magnitude as a function of parameters but remain size independent distinguishes the many body localization from localization in three dimension where g is constant only in a narrow range of $g \sim 1$. However, the difference disappears in both localized and ergodic regimes where the conductance becomes a fast function of the size.

Model. A good and physically realizable model is provided by the idealized Josephson junction chain with a high ratio of Josephson, E_J and charging energies E_C ,

$E_J \gg E_C$:

$$H = E_J \sum_{i=1}^L \cos(\phi_i - \phi_{i+1}) + E_C \sum_{i=1}^L (\hat{q}_i - n_i)^2, \quad (1)$$

where \hat{q} is the operator conjugated to the phase, n is the random static offset charge. In this system the localization transition is driven by temperature and becomes very high at large E_J : $T_{MBL} \sim E_J^2/E_C$ [5]. On the other hand, in the whole range $T \gg E_J$ the classical dynamics of the phase is only weakly affected by the Josephson couplings and is almost periodic indicating that the system is non-ergodic in this regime. For numerical analysis reported here we have restricted the allowed charging states by $-Q \leq q \leq Q$ with $Q = 2$. This restriction allows one to define the limit of infinite temperatures. Because in a physical chain ($Q = \infty$) at temperature $T_{ph} \gg E_C$ the average charge is large but finite, $\langle q^2 \rangle = T_{ph}/E_C$, the limit of infinite temperature of the model with finite Q corresponds to $T_{ph} \sim Q^2 E_C$ of the physical chain [5]. We assume that n is distributed uniformly in the interval $(-W/2, W/2)$ and focus on the regime of relatively strong disorder $W = 10$. Note that while in the realistic chain the offset charges n are completely random, their effective range is $-1/2 \leq n \leq 1/2$ because larger n can be eliminated by the shift of q . In the model with restricted $-Q \leq q \leq Q$, this is not true and the range of n becomes relevant.

Results. We perform the exact diagonalization of the restricted model (1) and analyze a few states at energies $E = E_{gs} + \bar{\epsilon} * (E_{max} - E_{gs})$, where E_{max} , E_{gs} are the largest and smallest eigenstate of the system, respectively to compute Thouless energy. We define density-density correlator near energy E by

$$K_E(\omega) = \frac{N^2 \sum_{\alpha, \beta} |\psi_{\alpha}(i)|^2 |\psi_{\beta}(i)|^2 \delta(E_{\alpha} - E_-) \delta(E_{\beta} - E_+)}{\sum_{\alpha, \beta} \delta(E_{\alpha} - E_-) \delta(E_{\beta} - E_+)} \quad (2)$$

where N is the dimension of Hilbert space, $E_{\pm} = E \pm \omega/2$, $\psi_{\alpha}(i)$ is the wavefunction at site i in the Fock space of charge quantum numbers, the bar means average over all different charge states and disorder realizations. The result of the computation is shown in Fig. 2 for the intermediate values of E_J . Two features are remarkable: $K_E(\omega)$ has a power law dependence in a wide frequency interval $E_{Th} < \omega < \delta$: $K_E(\omega) \sim N^{\beta} \omega^{-\mu}$ and the exponents of this power law are non-trivial ($\mu \approx 0.4$, $\beta \approx 0.3$). Such behavior indicates that at small ω K is dominated by the collective states formed by the resonances that form a mini band. The correlation between these state slowly drops as ω is increased. In fact, this behavior can be reproduced by the fractal random local spectrum similar to the Cantor set, namely, the spectrum in which the distances between levels, Δ are random independent

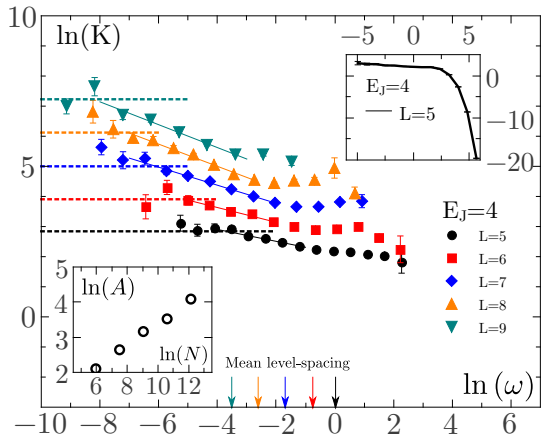


FIG. 2. Logarithm of density-density correlations, $\ln(K_E)$, as a function of the logarithm of the energy, $\ln(\omega)$, in the multifractal regime, $E_J = 4$. Each data set corresponds to a different system size L . The arrows indicate mean-level spacing, δ , for each of the sizes. Partial diagonalization is used to compute $\ln(K_E)$ with a few eigenstates at energy density $\bar{\epsilon} = 0.1$ in the main panel. The solid lines are fits $\ln K_E = \ln A - \mu \ln \omega$ that gives $\mu = 0.20, 0.25, 0.30, 0.36, 0.38$ for $L = 5, 6, 7, 8, 9$ respectively. The dotted horizontal lines represents $\ln(N \langle I_2 \rangle / 3)$, where $I_2 = \sum_i |\psi_\alpha(i)|^4$ and $\langle \dots \rangle$ denotes average over different samples. Inserts: (top) the dependence $\ln(K_E(\omega))$ in the whole range of ω obtained from full diagonalization for $L = 5$ and (bottom) $\ln A$ as a function of $\ln(N)$.

variables with power law distribution:

$$P(\Delta) = C \frac{\delta^{D_s}}{\Delta^{1+D_s}}, \quad \Delta > \delta, \quad (3)$$

where $C \sim 1$ and δ gives the low energy cutoff [23]. The spectrum of energy levels with spacing distributed according to (3) contains large gaps and dense regions, zoom into a dense region shows that it contains gaps and denser regions in its turn, see Fig. 1. Power law distribution of energy spacing translates into the power dependence $K(\omega) \sim N^\beta \omega^{-\mu}$ with two independent exponents, β and μ that are related to D_2 and D_s by $\beta = D_s - D_2$ and $\mu = 1 - D_s$ (see computation in Supplementary material). The fractal structure of the local spectrum implies that in this regime the wave function is first spread over a small cluster of close resonances, these resonances are weakly entangled with another cluster further away to form a supercluster, etc and form large scale hierarchical structure similar to spin glasses.

The data shown in Fig. 2 and similar ones for different E_J can be used to compute the Thouless energy that we define as the energy at which power law of $K(\omega)$ saturates at small ω [24]. In order to avoid direct computation of $K(\omega)$ at small frequencies we have used the result for the participation ratio $I_2 = \sum_i |\psi_\alpha(i)|^4$. At very small frequencies one expects that $K(\omega) \rightarrow c' I_2$ where $c' \sim 1$. For Gaussian random matrix $c' = 1/3$, we shall use this value because it agrees very well with the results of the compu-

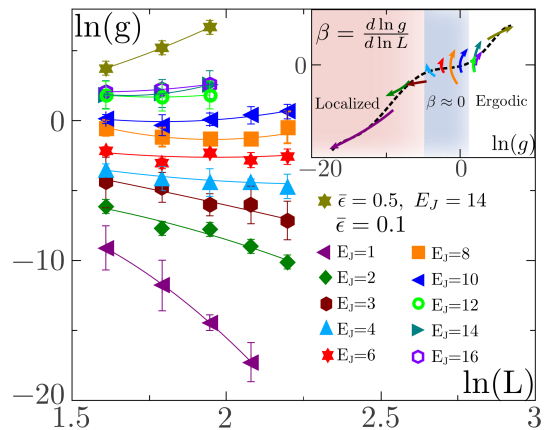


FIG. 3. Logarithm of the effective 'conductance', $g = E_{Th}/\delta$, as a function of the system size, L . The uppermost curve in the main panel has been computed at the middle of the band, $\bar{\epsilon} = 0.5$. All other curves correspond to the energy $\bar{\epsilon} = 0.1$. The insert shows the β function computed from these data. The dotted line is a fit of all the β functions for different sizes to a 5th order polynomial.

tation at small sizes L for which we were able to compute $K(\omega)$ for small ω directly. Combining the asymptotic at very small frequencies with the power law dependence at $\omega < \delta$ we determined the crossover frequency, E_{Th} and the effective 'conductance' of the many body problem, $g = E_{Th}/\delta$ shown in Fig. 3.

The size dependence of the effective conductance displays three distinct regimes. For $E_J \lesssim 3$ it decreases exponentially with the system size, similar to localized regime in conventional single particle theory. The critical value $E_J \approx 3.5$ coincides with one found for full many body localization from level statistics. Notice that the decrease of $g(L)$ disappears already for $g > 10^{-2}$, at larger g one does not observe any noticeable size dependence. Only at much larger $g \gtrsim 10$ (realized at $E_J \gtrsim 8$), exponential increase with the system size is observed, signaling the appearance of conventional ergodic state. This result is in a sharp contrast with three dimensional localization in which the conductance varies exponentially with the system size for small g and power law in system size for large g . This difference is due to the fact that in three dimensions the probability to find the energy level within the interval ΔE from the one at the origin increases as a power of the distance $\nu \Delta E L^3$ whereas the tunneling amplitude decreases exponentially if it is smaller than one. Because conductance at size L is proportional to the tunneling amplitude at this size, at small conductance $g < g_c \sim 1$ the virtual processes in which the particle hops to the state close in energy in order to cross the sample of size L become irrelevant. In many body system the number of states grows exponentially with the number of steps, so it has a chance to compensate the decrease in the tunneling amplitude even for

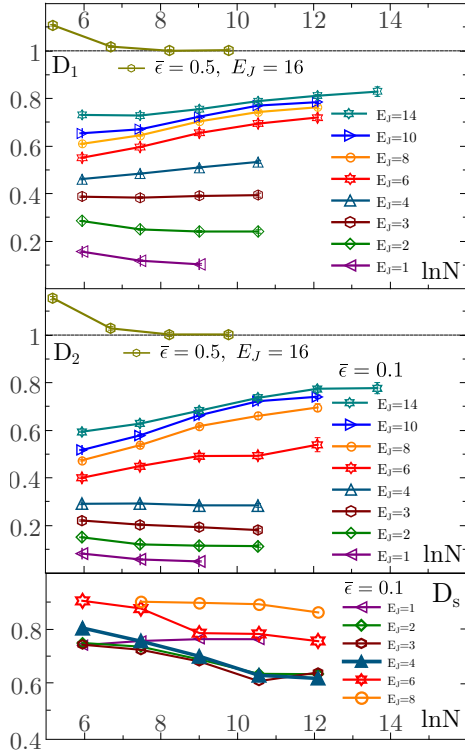


FIG. 4. Fractal dimensions (D_1 , D_2 and D_s) as a function of logarithm of Many-Body space. Each data set corresponds to a given value of Josephson coupling E_J . Energy density is $\bar{\epsilon} = 0.1$ for all points except one which corresponds to the middle of the spectrum $\bar{\epsilon} = 0.5$.

small g .

This existence of the intermediate nonergodic regime for $3 \lesssim E_J \lesssim 8$ is in a full agreement with the analysis of the wave function moments, defined by $I_q = \sum_i |\psi(i)|^{2q}$ at the energy density $\bar{\epsilon}$. The power law dependence $I_q \sim N^{-D(q-1)}$ implies that the wave function has fractal dimension D . In a multifractal system the dimension D acquires dependence (usually small) on q . The most important for physical properties are the first moments D_1, D_2 defined for the finite systems by

$$D_q = \frac{1}{q-1} \frac{d \ln I_q}{d \ln N}, \quad (4)$$

with the case $q = 1$ is understood as a limit $q \rightarrow 1$.

We have computed dimensions D_1 and D_2 by using the discrete version of Eq. 4 for the eigenstates of Hamiltonian in Eq. 1. The data from sizes $L+1$ and $L-1$ has been used to compute $D_q(L)$:

$$D_q(\ln N) = \frac{1}{q-1} \frac{\Delta \ln \bar{I}_q}{\Delta \ln N}, \quad (5)$$

where bar denotes average over disorder realizations. In Fig. 4, D_q is shown as a function of the logarithm of configuration space $\ln(N)$ for different Josephson coupling ranging from $E_J = 1$ to $E_J = 14$.

For very small $E_J \lesssim 2$, fractal dimensions definitely decrease with the increase of system size in Fig. 4. However the size dependence becomes very weak in a wide range of $2 \lesssim E_J \lesssim 14$. Notice that even for largest studied E_J one does not observe clear saturation at $D_2 = 1$. Instead, at $E_J = 14$ the saturation corresponds to $D_2 \approx 0.8$, reminding of the behavior of D_2 in random regular graphs. Only at large E_J and energy in the middle of the spectrum, the data are consistent with dimensions $D_1 = D_2 = 1$. The apparent absence of saturation at $D_1 = D_2 = 1$ for $\bar{\epsilon} = 0.1$ might be due to the fact that the small value of the energy density suppress the amplitude of the wave functions corresponding to large charging energy states. However, this mechanism seems unlikely for large $E_J \gg QE_C$ that are sufficient to mix all charging states. The range of E_J ($2 \lesssim E_J \lesssim 14$) in which one observes size independent anomalous dimensions should be compared with the results of the spectra analysis that indicate full transition at $E_J \approx 3.5$. The fact that full MBL occurs close to the lower boundary of the range is difficult to reconcile with the alternative explanation that attributes size independence of D to the finite size effects around the critical point. Finally, we note that the multifractality is strong in the range $E_J = 4$ to $E_J = 6$, as D_1 is significantly larger than D_2 .

Conclusion. Our results confirm the existence of the multifractal regime in the interval $3 \lesssim E_J \lesssim 8$ for the model (1) of the Josephson junction chain in agreement with previous findings [5]. In this regime both the local energy spectrum and spacial structure are fractal. The scaling behavior is characterized by size independent generalized many body conductance that varies by orders of magnitude as a function of E_J . This finding is hardly compatible with the single parameter scaling because it leads to a very abnormal $\beta = d \ln g / dL$ function shown in Fig. 3. The appearance of a strange regime in which $\beta \approx 0$ for all sizes is a clear evidence for the new genuine phase, a “bad” metal. Physically, in this phase one observes some dissipation and transport but everything is slow and thermodynamic equilibrium is never reached. We notice that violation of single parameter scaling has recently been found in the metallic side of Random-Regular graph [25]. We also notice that the soluble 1D model that exhibits similar behavior due to exact conservation laws was proposed recently in [26]. Similar to Josephson chain, the number of states per site in this model is larger than 2 which indicates that absence of non-ergodic regime claimed in some previous works [19, 21, 27] might be due to the choice of the model with only 2 states per site in 1D chain. Alternative point of view is that Hilbert space sizes available for exact numerical diagonalization are always too small to get out of the critical regime [14]. The observation of the fractal structure of the local spectra allows to resolve this controversy by studying the local spectra by real space renormalization group technique.

Acknowledgment. This work was supported by ARO grant W911NF-13-1-0431 and Russian Science Foundation 14-42-00044. M. P. acknowledge support from Juan de la Cierva IJCI-2015-23260, MINECO/FEDER Project FIS2015-70856-P and CAM PRICYT Project QUITEMAD+ S2013/ICE-2801.

-
- [1] P. W. Anderson, Phys. Rev. **109**, 1492 (1958).
 - [2] G. Feher, Phys. Rev. **114**, 1219 (1959).
 - [3] D. Basko, I. Aleiner, and B. Altshuler, Annals of Physics **321**, 1126 (2006).
 - [4] F. Evers and A. Mirlin, Reviews of Modern Physics **80**, 1355 (2008).
 - [5] M. Pino, L. B. Ioffe, and B. L. Altshuler, Proceedings of the National Academy of Sciences **113**, 536 (2016).
 - [6] Y. Bar Lev and D. R. Reichman, Phys. Rev. B **89**, 220201 (2014).
 - [7] D. J. Luitz, N. Laflorencie, and F. Alet, Phys. Rev. B **93**, 060201 (2016).
 - [8] D. J. Luitz and Y. Bar Lev, preprint arXiv:1702.03929 (2017).
 - [9] M. Schreiber, S. S. Hodgman, P. Bordia, H. P. Lüschen, M. H. Fischer, R. Vosk, E. Altman, U. Schneider, and I. Bloch, Science **349**, 842 (2015).
 - [10] A. De Luca, B. L. Altshuler, V. E. Kravtsov, and A. Scardicchio, Phys. Rev. Lett. **113**, 046806 (2014).
 - [11] B. L. Altshuler, E. Cuevas, L. B. Ioffe, and V. E. Kravtsov, Phys. Rev. Lett. **117**, 156601 (2016).
 - [12] G. Biroli, G. Semerjian, and M. Tarzia, Progress of Theoretical Physics Supplement **184**, 187 (2010).
 - [13] B. L. Altshuler, Y. Gefen, A. Kamenev, and L. S. Levitov, Phys. Rev. Lett. **78**, 2803 (1997).
 - [14] K. S. Tikhonov and A. D. Mirlin, Phys. Rev. B **94**, 184203 (2016).
 - [15] C. L. Bertrand and A. M. Garcia-Garcia, Phys. Rev. B **94**, 144201 (2016).
 - [16] F. L. Metz and I. P. Castillo, arXiv:1703.10623 (2017).
 - [17] K. Agarwal, S. Gopalakrishnan, M. Knap, M. Müller, and E. Demler, Phys. Rev. Lett. **114**, 160401 (2015).
 - [18] S. Gopalakrishnan, K. Agarwal, E. A. Demler, D. A. Huse, and M. Knap, Phys. Rev. B **93**, 134206 (2016).
 - [19] M. Serbyn and J. E. Moore, Phys. Rev. B **93**, 041424 (2016).
 - [20] X. Deng, B. L. Altshuler, G. V. Shlyapnikov, and L. Santos, Phys. Rev. Lett. **117**, 020401 (2016).
 - [21] M. Serbyn, Z. Papić, and D. A. Abanin, arXiv preprint arXiv:1610.02389 (2016).
 - [22] E. Cuevas and V. E. Kravtsov, Phys. Rev. B **76**, 235119 (2007).
 - [23] V. Kravtsov and A. Scardicchio, unpublished.
 - [24] V. E. Kravtsov, I. M. Khaymovich, E. Cuevas, and M. Amini, New Journal of Physics **17**, 122002 (2015).
 - [25] I. Garcia-Mata, O. Giraud, B. Georgeot, J. Martin, R. Dubertrand, and G. Lemarie, preprint arXiv:1609.05857 (2016).
 - [26] A. Smith, J. Knolle, D. L. Kovrizhin, and R. Moessner, preprint arXiv:1701.04748 (2017).
 - [27] M. Schiulaz, A. Silva, and M. Müller, preprint arXiv:1410.4690 (2014).
 - [28] V. Oganesyan and D. Huse, Physical Review B (Condensed Matter) **75**, 155111 (2007).
 - [29] E. Cuevas, M. Feigel'man, L. Ioffe, and M. Mezard, Nature Communications **3**, 1128 (2012).
 - [30] Y. Y. Atas, E. Bogomolny, O. Giraud, and G. Roux, Phys. Rev. Lett. **110**, 084101 (2013).
 - [31] R. B. Lehoucq, D. C. Sorensen, and C. Yang, *ARPACK users' guide: solution of large-scale eigenvalue problems with implicitly restarted Arnoldi methods*, Vol. 6 (Siam, 1998).
 - [32] D. J. Luitz, N. Laflorencie, and F. Alet, Phys. Rev. B **91**, 081103 (2015).

Supplementary material

STATISTIC OF EIGENENERGIES

We present additional numerical results that allow us to establish the position of the full MBL phase transition. We have computed the ratio of consecutive eigenenergies $r = \min(\delta_i, \delta_{i+1}) / \max(\delta_i, \delta_{i+1})$, where $\delta_n = E_{i+1} - E_i$ [28, 29]. We expect $\langle r \rangle = 0.536$, for Wigner-Dyson distribution and $\langle r \rangle = 0.386$ in for Poisson distribution [30]. At finite system sizes, a crossing point for curves with different sizes would indicate the location of the Many-Body Localization transition.

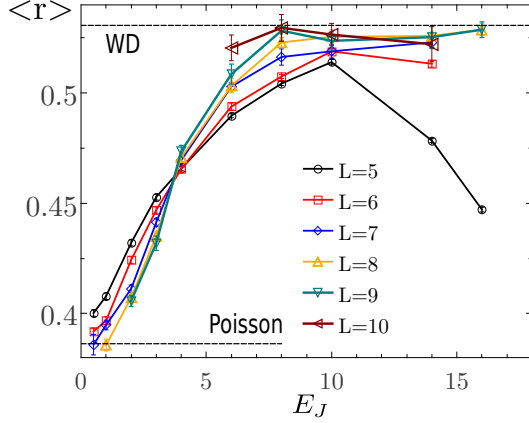


Fig. SI 1. Ratio of minimum and maximum consecutive eigenenergies difference, $r = \min(\delta_i, \delta_{i+1}) / \max(\delta_i, \delta_{i+1})$, for eigenenergies at energy $\bar{\epsilon} = 0.1$. Sizes run from $L = 5$ to $L = 10$, as indicated in the legend. The horizontal lines represent the value of $\langle r \rangle$ for Gaussian Orthogonal ensemble $\langle r \rangle = 0.536$ and for Poisson $\langle r \rangle = 0.386$.

Fig. SI1, gives $\langle r \rangle$ for levels at energy $\bar{\epsilon} = 0.1$ as a function of E_J for several sizes $L = 4, 5 \dots 10$. One observes that spread of the curves at $E_J \gtrsim 3.5$ similar to the behavior expected above the crossing point $E_J \approx 3.5$. Because at $E_J \lesssim 3.5$ the $g(\ln L)$ dependence shows the insulating behavior, one is tempted to identify this point with the full many body localization. However, at $E_J \lesssim 3.5$ the curves for larger sizes overlap indicating that the level repulsion does not completely disappear in this regime. Furthermore, the anomalous dimensions at $E_J \lesssim 3.5$ do not show the convergence to 0, so we can only conclude that the transition to full many body localization occurs

at $E_J \leq 3.5$ in this model.

FRACTAL ENERGY SPECTRUM

Here we compute the correlator $K(\omega)$ in the toy model of random fractal energy spectrum and show that it is given by $K(\omega) \sim N^\beta \omega^{-\mu}$. For each site, i , one can divide the wave functions into two groups: group I that includes site i in its support set and group II that does not. In the toy model we assume that the wave function amplitudes of group I are all large $|\psi_a(i)|^2 \sim M^{-1}$ while the amplitudes of wave functions in group II can be neglected. Here $M = N^{D_s}$ is the volume of the support set. Normalization condition implies that the total number of wave functions in group I is M . Furthermore, we assume that the spacings between energies of the energies of group I are given by

$$P(\Delta) = C \frac{\delta^{D_s}}{\Delta^{1+D_s}}, \quad \Delta > \delta. \quad (6)$$

where $1 < D_s < 0$ is the measure of the fractality of the local spectrum and $C \sim 1$.

Notice that this distribution of the spacings coincides with the one of the regular Cantor set for which fractal dimension $D_s = \ln 2 / \ln 3$.

In this model the $K(\omega)$ is given by the sum over all state in group I, each state giving contribution $1/M$:

$$K(\omega) = M^{-2} \sum_{a,b'} \delta(\omega - E_{ab}), \quad (7)$$

where $E_{ab} = \sum_{n=b}^a \Delta_n$. Notice that this model neglects factors of $N / \sum_{\alpha} \delta_{\alpha}(\omega - E_{\alpha})$ that have weak N -dependence. Introducing the Fourier transforms:

$$k(t) = \int K(\omega) e^{-i\omega t} d\omega$$

$$p(t) = \int P(\Delta) e^{-i\omega t} d\Delta.$$

For any distribution function its Fourier transform $p(0) = 1$, $\Re p(t \neq 0) < 1$ and $p(t \rightarrow \infty) = 0$. In addition, the power law distribution function (6) is given by $1 - p(t) \sim (t\delta)^{D_s}$ for $\delta t \lesssim 1$. Transforming both sides of Eq.(7) we obtain:

$$k(t) = M^{-2} \sum_{a,b}^M \langle e^{-it \sum_{n=b}^a \Delta_n} \rangle$$

$$= M^{-1} \left[2\Re \frac{1}{1 - p(t)} - 1 \right] \quad (8)$$

where we neglected the terms proportional to $p(t)^M \ll 1$. Transforming back to the frequency space we get power law dependence

$$K(\omega) = C_1 \frac{\delta^{-D_s}}{M\omega^{1-D_s}}, \quad (N^{D_2/D_s}\delta > \omega > \delta) \quad (9)$$

that saturates at $\omega < \delta$.

Assuming $\delta = g/N$ and using $M = N^{D_2}$ we obtain for $N^{-1+D_2/D_s} > \omega > \delta$:

$$K(\omega) \sim \frac{N^\beta}{\omega^\mu}, \quad (10)$$

where

$$\beta = D_s - D_2, \quad (11)$$

$$\mu = 1 - D_s. \quad (12)$$

These equation should be compared with the ones for the critical point of 3D Anderson model, where the standard Chalker's scaling holds:

$$\mu = 1 - D_2, \quad (13)$$

so that $D_s = D_2$ which implies that the fractality has the same dimension in real space and in frequency space.

In general, for $\beta \neq 0$ we have a generalized Chalker's scaling:

$$\mu + \beta = 1 - D_2. \quad (14)$$

The model considered in this paper corresponds to $\beta > 0$ (see Fig.2).

Note also that the power-law Eq.(9) terminates both at small $\omega \sim \delta = b/N$ and at large $\omega > N^{-1+D_2/D_s}$. Since at $\beta > 0$ we have $D_2 < D_s$ the power law dependence should stop before the band-edge at $\omega \sim 1$ is reached, so that $K(\omega)$ exhibits a plateau in the intermediate frequency range. This plateau can be seen in Fig. 2.

NUMERICAL COMPUTATIONS

The methods employed in previous works [15, 21] to compute Thouless energy in the metallic ergodic state become very difficult to use close to the many body localization transition and in the insulating state. The reason is that in the latter regimes the Thouless energy becomes very small which implies the need to compute very close pairs of energy levels that is numerically difficult. Our approach avoids this problem and allows to obtain E_{Th} even in the insulating regime. The idea is to compute $K(\omega)$ in the scaling regime and $K(0)$ separately. Matching the scaling dependence of $K(\omega)$ with the plateau at low frequencies allowed us to compute even very small

Thouless energies at small E_J as demonstrated in Fig. SI2.

The numerical diagonalization of Hamiltonian Eq. (1) has been done by two methods. In the first one, we have used partial diagonalization to obtain 3 eigenstates at a given energy density with ARAPCK's shift invert mode [31, 32]. In the second one, we have used a full diagonalization to obtain all the eigenstates. The former method has allowed the computation of system with sizes up to $L = 11$, while the last one is only capable of solving sizes up to $L = 8$. Full diagonalization has been employed to check the results of partial diagonalization for small systems and to obtain E_{Th} in the ergodic regime in which, Thouless energy is larger than mean level spacing, so one need to find eigenstates in a large energy interval to extract E_{Th} from $K(\omega)$. The number of disorder realization of Hamiltonian Eq. (1) used to average a given quantity has been chosen to make sensible error bars. Error bars are computed as the standard deviation of the population of measurements given by different realization of the disorder. We notice that smaller values of E_J requires larger number of disorder realizations. Thus, for $E_J \leq 4$, we have used around 10^4 realizations and for $E_J=14$ around 10^3 .

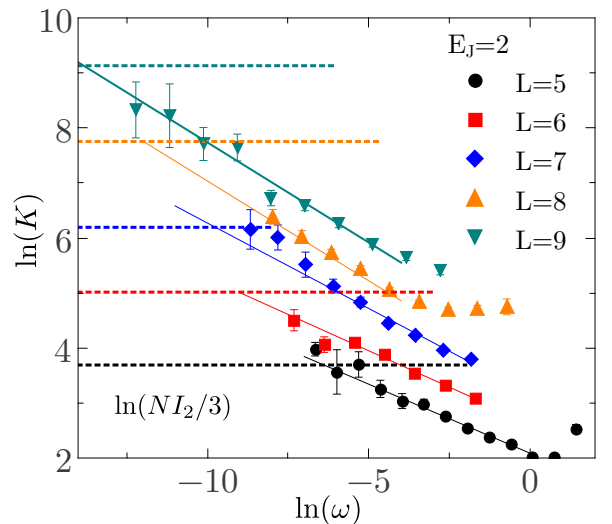


Fig. SI 2. $K(\omega)$ in the insulating regime ($E_J = 2$). The slope of the solid lines is $\beta \approx 0.4$. The dotted lines signals the value of $\ln(N I_2 / 3)$ for each of the sizes.